Sustainable Energy & Fuels

Dehydration of Highly Viscous Polyol (1,2,4-Butanetriol) Using Microwave-Induced Sweep Gas Membrane Distillation (MIMD) on Nanocarbon-Immobilized Membranes

Journal:	*Sustainable Energy & Fuels*
Manuscript ID	SE-ART-03-2025-000319.R1
Article Type:	Paper
Date Submitted by the Author:	31-May-2025
Complete List of Authors:	Chandra Bhoumick, Mitun; New Jersey Institute of Technology Harvey, Benjamin; Naval Air Warfare Center Weapons Division, Research Chemistry Zhang, Derek; Naval Air Warfare Center Weapons Division, Research, Chemistry Div. Mitra, Somenath; New Jersey Institute of Technology, Chemistry and Environmental Science

Dehydration of Highly Viscous Polyol (1,2,4-Butanetriol) Using Microwave-Induced Sweep Gas Membrane Distillation (MIMD) on Nanocarbon-Immobilized Membranes

Mitun Chandra Bhoumick[1], Benjamin G. Harvey[2], Derek D. Zhang[2], Somenath Mitra[1,*]

[1] Department of Chemistry and Environmental Science, New Jersey Institute of Technology, Newark, NJ 07102, USA

[2] US Navy, Naval Air Warfare Center, Weapons Division, Research Department, Chemistry Division, China Lake, CA 93555, USA

[*] Corresponding Author: Tel: 973-596-5611; Email: *Somenath.mitra@njit.edu*

Abstract

A challenge facing the synthesis of bioderived platform chemicals such as polyols and polyacids via fermentation processes is their separation from dilute aqueous streams. This study presents microwave-induced membrane distillation (MIMD) as a method for concentrating viscous 1,2,4-butanetriol (BT) at concentrations that can be sourced from fermentation broth. MIMD and sweep gas membrane distillation (SGMD) processes were employed to concentrate BT feed solutions utilizing nanocarbon-based membranes, namely carbon nanotube immobilized membrane (CNIM) or graphene oxide immobilized membrane (GOIM). Microwave heating (MWH) was utilized to elevate the temperature of the feed system and was found to be superior to conventional heating (CH) in terms of flux, mass transfer coefficients and thermal efficiency. Our findings reveal that GOIM membranes exhibited an 11.5% higher dehydration rate compared to CNIM membranes. Initial water flux reached 14.1 kg/m²h, albeit this value decreased thereafter as the concentration of BT increased, thus limiting mass transfer coefficients due to increased viscosity, which reached to 11.41 mPa.s at 90 wt.% and 80 ℃. Overall, MWH substantially alleviated this issue, leading to a flux as high as 15.7 kg/m^{2}h and a 35% improvement in mass transfer coefficients over CH. The overall thermal efficiency of BT concentration reached 74.5% for GOIM-based MIMD with a specific energy consumption (SEC) of 263 kWh/m^3, which showed a 6.5% reduction compared to CH.

Keywords:1,2,4-butanetriol, Microwave-induced membrane distillation, Dehydration

1. **Introduction**

Platform chemicals, also known as building block or bulk chemicals, are intermediate compounds that serve as key precursors to produce a variety of end-use materials such as plastics, fibers, pharmaceuticals, and other specialty chemicals [1-3]. Currently the US Department of Energy is emphasizing the synthesis of platform chemicals such as polyacids and polyols from renewable resources via processes such as fermentation. 1,2,4-Butanetriol (BT) is such a polyols intermediate serving as a foundational component for a wide array of applications such as controlled drug release, a plasticizer for polymers like polyurethane [4-5], a precursor for propellent and antiviral pharmaceutical compounds. Commercial production of BT involves the hydrogenation of D,L-malic acid esters [6-7] . However, this method generates a significant waste stream and is expensive due to the use of $NaBH_4$ as a stoichiometric reducing agent.

There is a growing interest in exploring alternative biosynthetic approaches for BT production [8-12]. These include a four-step enzymatic reaction using xylose as a substrate [13-14], and a two-step fermentation strategy utilizing *Pseudomonas fragi* and recombinant *Escherichia coli* [14-15]. In addition, there are ongoing efforts to streamline BT production into a single-step process by introducing enzymes into a recombinant E. coli strain. However, bio-based fermentation products are typically obtained as components of complex aqueous solutions. Isolation of BT can be complicated by low BT concentration (2 - 4%), and a complex array of contaminants including bacteria, proteins, polysaccharides, monosaccharides, polyols, organic acids, and inorganic salts [5, 16]. Moreover, BT's polyhydroxy structure results in strong hydrophilicity and a high boiling point rendering the separation and purification of bio-based BT challenging [17-19]. Consequently, the substantial separation costs account for over 70% of total production expenses, significantly hinder large-scale bio-based BT production. Various traditional separation methods such as distillation, adsorption, aqueous two-phase extraction, and reactive extraction have been explored for

polyalcohol recovery [4, 15]. These processes have been limited in terms of yield, selectivity, and cost.

Membrane-based purification methods such as membrane distillation (MD) could be a potential approach to enrich BT from the fermentation broth [20-21]. MD is a thermal separation technique used to purify and concentrate liquids, especially aqueous solutions, by exploiting vapor pressure differences across a hydrophobic membrane [22-25]. A hot feed is brought into contact with one side of a porous hydrophobic membrane, while a cooler or a lower-pressure environment is maintained on the other side [22-29]. As the solution heats up, water molecules evaporate and go through the membrane, leaving behind concentrated solute. The goal of such an MD process is to enhance the water removal, where the highly soluble BT may pose some challenges, and highly selective membranes are needed to provide rapid water removal [30-37]. The development of high flux carbon nanotube (CNT) and graphene oxide (GO) immobilized membranes represent a major advantage in such dewatering applications [38-41].

Recently we have reported the development of microwave-induced membrane distillation (MIMD), which is an innovative approach that combines microwave heating (MWH) with the MD process. Microwaves can rapidly heat the feed solution [34, 42] and specifically target polar molecules that are microwave active. In MD, this selective heating can promote the vaporization of the volatile component, facilitating its transfer through the membrane. Microwaves also lead to rotation and vibration of molecules which lead to breakdown of hydrogen-bonded structures encountered in aqueous environments, leading to higher flux and selectivity.

In this study, the goal is to use sweep gas membrane distillation (SGMD) to dehydrate BT from low concentration aqueous streams using high flux CNT and GO based membranes. Yet another objective is to test MIMD as an approach that may lead to energy saving and increased

flux over conventional heating (CH) because it is expected that hydrogen bonded BT-water clusters will be disrupted during MWH.

2. Materials and methods

2.1. Chemicals and materials

A flat-sheet polytetrafluoroethylene (PTFE) membrane with a polypropylene (PP) supporting layer (0.22 μm pore size, 119 μm thickness, and 74% porosity) was obtained from Adventec Toyo Kaisha, Ltd., (Tokyo, Japan). 1,2,4-Butanetriol (Fisher Scientific), and acetone (Millipore Sigma) were used as received. In all experiments, deionized (DI) water was used. Multi-walled carbon nanotubes (MWCNTs) and graphene oxide (GO) were purchased from Cheap Tubes Inc., Brattleboro, VT. The MWCNTs had an average utter diameter of ~30 nm and a length of 15 μm.

2.2. Membrane fabrication

The fabrication of carbon nanotube and graphene oxide membranes was carried out using a two-step process. In the first step, CNT and GO nanomaterials were efficiently dispersed in acetone using ultrasonication, following the methodology reported elsewhere [43-44]. A sonication bath (TRU-SWEEP TM Ultrasonic cleaner, CREST ULTRASONICS) was used to disperse the nanoparticles. Sonication time was set at 3 h. For each membrane, 0.75 mg of the nanomaterials were dispersed in 10 mL of acetone. In a separate vial, 0.1 mg of PVDF was mixed with 2 mL of acetone and sonicated to obtain a homogeneous solution, which was then added to the dispersed nanomaterials as a binder during the immobilization process. PTFE membranes were drop-coated

with the dispersed nanomaterial solutions and left to dry overnight under a hood at room temperature. Vacuum was applied to uniformly coat the PTFE membrane surface. The CNT immobilized membrane is labeled as CNIM and GO immobilized membrane is labeled as GOIM.

2.3. Characterization

Surface morphology for the CNIM and GOIM membranes was studied using a scanning electron microscopy (SEM, JEOL JSM 7900 Oxford Instruments). Contact angle (CA) for DI water and BT mixtures was measured by putting 5 μL droplet on the surface and calculating the angle by Image J software. The mean value of three replicates was reported. Membrane thickness was measured using a micrometer (Mitutoyo 293-340-30 Digital Micrometer). Average value of at least 3 readings was reported. Wetting resistance of the modified membranes was evaluated using a home-made liquid entry pressure (LEP) device similar to what has been reported before [43]. Pressure was increased step by step to see where the first liquid flow comes out of the membranes. The device is made of a nitrogen gas tank, dispensing pressure vessel (1 gallon in volume, Millipore Sigma) connected to a pressure gauge, a PP filter holder (47 mm effective area up to 5 bars, Cobetter Filtration) and a container to collect the liquid that passes through the membrane. Porosity of the fabricated membranes was measured using a gravimetric method as follows. Membranes were cut in a specific shape and weighed and then immersed in wetting liquid for at least 24 h. Then the wet weight of the membranes was measured using a digital analytical balance.

2.4. MIMD

The experiments were conducted in a bench-scale MD system and the setup for MIMD is shown in Figure 1. This setup was similar to an experimental system reported previously [35,43]. The

membrane module was made of PTFE round sheets. The hot feed entered the feed side of the module while the cool gas swept through the permeate side to remove the vapors. Insulated tubing was utilized to minimize heat loss during the experiments. The effective membrane surface area used in the experiments was 11.80 cm^2. To circulate the hot feed, a peristaltic pump (Cole Parmer, model 77200-52) was used, and its temperature was regulated by a water bath. The feed and permeate temperatures were monitored using K-type temperature sensors. Dry laboratory air was used as the sweeping gas during the experiments. The sweeping gas flow rate was set to be 2 mL/min throughout the tests. The change in feed weight was measured using a digital scale (with two decimal point accuracy). An enclosed feed chamber was used to ensure that there was no feed loss during the experiment. The concentration of BT was measured using a refractive index meter (Cole-Parmer Digital Refractometer, 0 - 85% Brix, 1.3330 - 1.5100 RI). The experiments were repeated three times, and the relative standard deviation was below 5%.

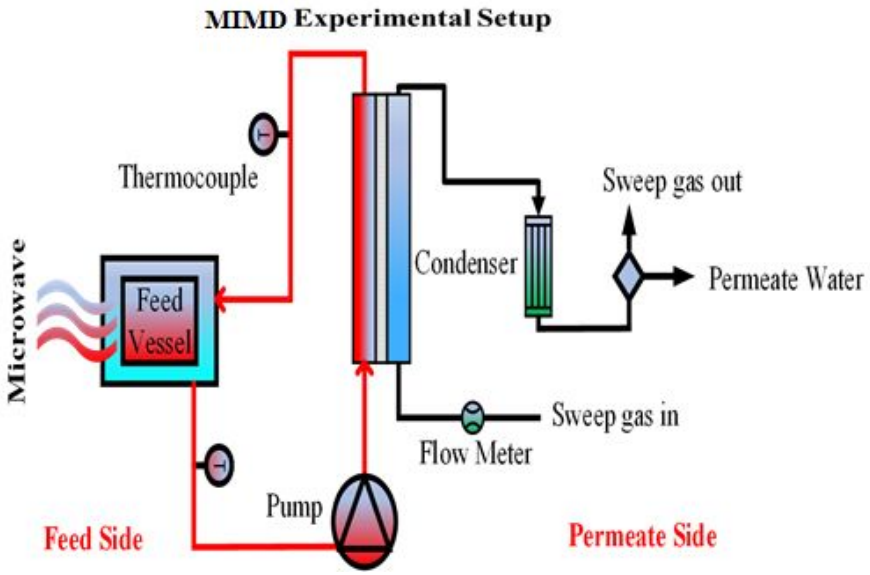

Figure 1: Experimental setup for the dehydration of BT using microwave heated SGMD.

2.5. Viscosity Measurements

At high concentrations, the BT mixtures became viscous and dense. All viscosity and density measurements were obtained with an Anton Parr SVM 3001 Cold Flow Properties Viscometer. Temperature was regulated using an internal Peltier heating and cooling system alongside a Julabo FP50-HL heating and cooling circulator. All samples were prepared by mixing BT with water by mass. Concentrations of 70 - 90 wt.% BT were measured normally on the viscometer at 80 °C. 10 - 60 wt.% BT mixtures could not be measured normally at 80 °C, potentially due to bubble formation. Instead, the 10 - 60 wt.% samples were ramped from 20 °C up to a final temperature as close to 80 °C as possible with data points taken every 5 °C. The density values were then extrapolated via linear regression to provide densities at 80 °C. Kinematic viscosity data were modeled using Microsoft Excel's exponential regression and viscosity values at 80 °C were obtained by extrapolation for the 10 - 60 wt.% BT mixtures.

3. Results and Discussion

3.1. Membrane characterization

The SEM images for GOIM and CNIM are shown in Figure 2. The nanocarbons are well dispersed with intact pore structures. Table 1 summarizes membrane properties for CNIM and GOIM. The incorporation of GO and CNT altered the CA compared to the control membrane. Membranes showed high hydrophobicity toward DI water and these angles decreased as the BT concentration increased. Surface tension for water (~72 mN/m) is higher than that of BT (~50 mN/m) and this caused the BT mixtures to wet the membrane surface easier than the DI water as the concentration of BT increased in the mixture. The loading of nanocarbon was kept the same for both the membranes. Using DI water, LEP was found to be 62 and 65 psi for the GOIM and

CNIM membranes, respectively. Having higher LEP translated into more wetting resistance and more secure operation in longer operating time. It means that the larger pores on the membrane surface will not get wet easier in contact with the feed.

Table 1. Physical properties for CNIM and GOIM Membranes.

Membrane	Nanocarbon loading (mg/cm^2)	CA (°)				Porosity (%)	LEP (psi)	Thickness (μm)
		DI water	25 wt.% BT	50 wt.% BT	100 wt.% BT			
GOIM	0.06	117 ± 2	101 ± 2	89 ± 2	78 ± 2	73 ± 0.02	62 ± 3	133 ± 3
CNIM	0.06	126 ± 2	110 ± 2	96 ± 2	82 ± 2	73 ± 0.02	65 ± 2	135 ± 2

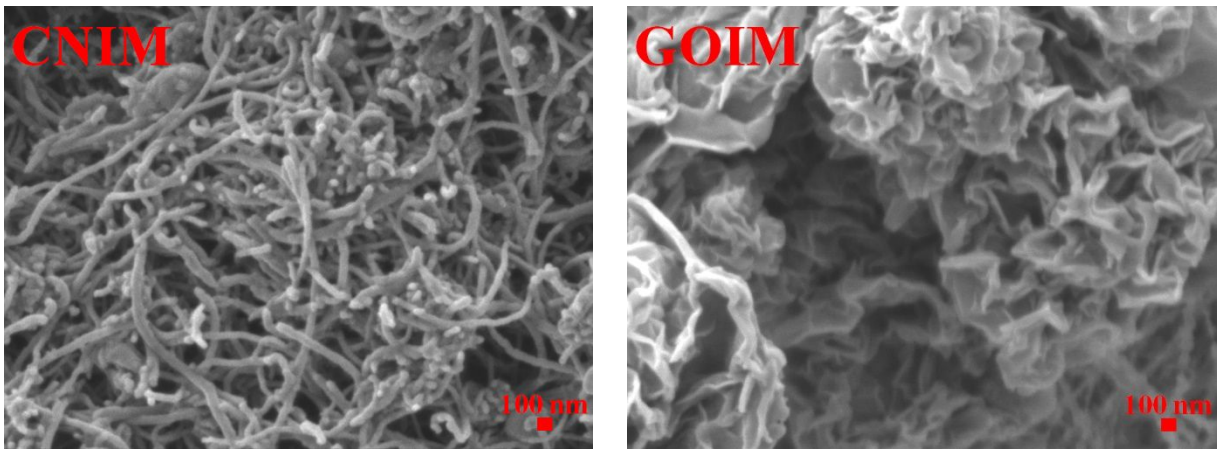

Figure 2: Surface SEM images of the CNIM and GOIM membranes. The scale bar is 100 nm long. The magnification is 30 kx for the SEM images.

3.2. Dehydration using CNIM and GOIM

The Antoine equation was used to determine the vapor pressure at a temperature range of 340-390 °K for the BT-water mixtures. In Figure 3, the vapor pressure as a function of temperature is shown for the pure compounds. The vapor pressure of water and BT is important during the membrane distillation process. The separation of the two components and the water flux depends on the vapor pressure gradient. The formula for the Antoine equation is shown in Eq. 1 as follows:

$$\text{Log}_{10}(P) = A - (B/(T + C)) \quad \text{..... (1)}$$

Antoine equation constants for 1,2,4-butanetriol were not available and the constants for 1,2,3-butanetriol instead, which we believe is a fair assumption. The Antoine parameters for BT are as follows: A (6.766), B (3681.25) and C (6.727). Similarly, the Antoine parameters for water are A (8.07), B (1730.63), and C (233.426). From the figure, it is evident that the vapor pressure of water is increasing exponentially with respect to temperature. Meanwhile, at the temperatures studied, the vapor pressure of BT is negligible as these compounds have significantly different boiling points (~300 ℃ at 1 atm versus 100 ℃ at 1 atm). Therefore, it is anticipated that during membrane distillation, the water would be more prominent in the permeate side compared to BT.

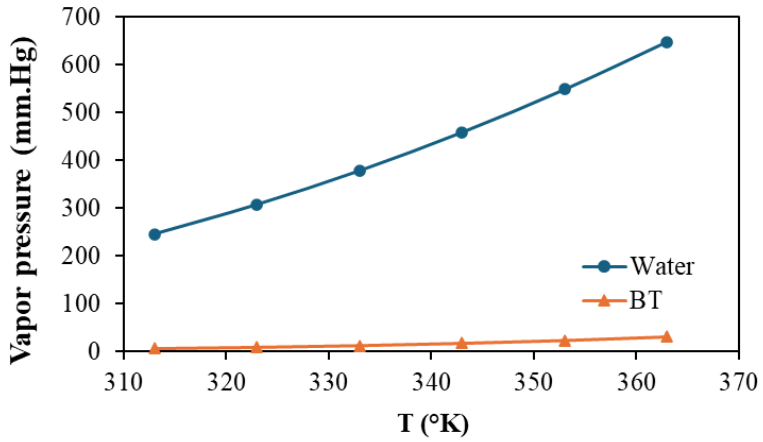

Figure 3. Vapor pressure of BT and water as a function of temperature using the Antoine equation.

The dehydration efficiency of aqueous BT mixtures was examined by measuring the concentration of BT before and after the MD tests using both CH and MWH methods. Various operating parameters were adjusted and their correlation with experimental findings was analyzed. Additionally, the mass transfer coefficient was assessed by measuring concentration as a function of time during the dehydration process. The amount of water permeating through the membrane was calculated from the measured water concentration in the permeate and the weight of collected permeate. The efficiency of separation for each membrane studied was determined by measuring the final concentration of the feed. The higher the concentration of the feed after the experiments, the higher the process efficiency.

The water flux for SGMD of an aqueous BT solution is shown in Figure 4. Here, CH and MWH were applied and compared with respect to water flux. Both GOIM and CNIM membranes were used for the performance study. At 80 °C using CH, the average flux for CNIM and GOIM

was 13.8 ± 0.53 kg/m^{2}h and 14.7 ± 0.69 kg/m^{2}h, respectively. Therefore, GOIM was more permeable than CNIM.

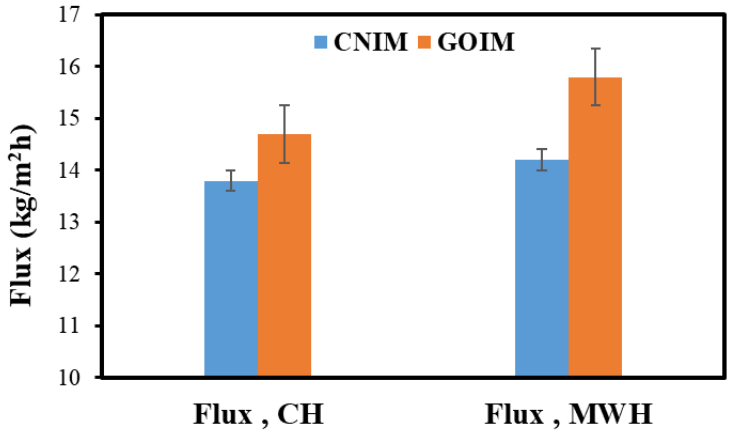

Figure 4. Average water flux for a 5 wt.% aqueous BT mixture at 80 °C and a flowrate of 100 mL/min.

The enrichment of BT depends on the efficient removal of water as a permeate in the membrane distillation process. MIMD showed some unique advantages in water removal. When subjected to microwave radiation, water and BT exhibited distinct behaviors due to differences in dielectric constant, heating rate, and boiling point. Both water and BT are polar molecules and microwaves induce rotations/vibrations that generate heat via molecular friction. Despite their similar polar characteristics, water, with its higher dielectric constant (κ = 78.4) absorbs microwave energy more effectively than BT (κ = 32). Consequently, water experiences faster heating and reaches its lower boiling point before BT. Also, MWH is known to facilitate the disruption of hydrogen bonded water-organic clusters which will further facilitate water removal

[42]. Finally, the Antoine equation illustrates the subtle increase in vapor pressure for BT compared to water, which results in its concentration during MD.

The concentration of BT in the feed was a critical factor in determining the flux due to the high viscosity of BT. The microwave induced breakdown of clusters enhanced mass transfer processes, but increased viscosity reduced mass transfer. Figure 5-A illustrates the gradual decline of water flux as a function of feed concentration. The feed without BT showed the highest flux for both CNIM and GOIM membranes using conventional and MWH. Increasing the concentration of BT in the feed reduced the overall flux with respect to time. Initially the flux drop was relatively slow compared to the increase in BT concentration. However, flux steadily dropped as the concentration increased to 20 wt.%, after which flux decreased exponentially. For example, the flux dropped from 15.8 kg/m^{2}h to 10.4 kg/m^{2}h for the GOIM membrane with MWH as the concentration changed from 5 to 57 wt.%. The lowest flux was seen in the case of the CNIM membrane with CH. As the water content in the feed side dropped, the viscosity of the solution increased. As a result, less water vapor was formed, resulting in a lower vapor pressure.

Figure 5-B represents the concentration of BT in the feed with respect to SGMD operating time. The experiment was conducted for 13 h and concentration was measured hourly. The initial concentration was 20 wt.%, and the flowrate was maintained at 100 mL/min with a feed temperature of 80 °C. A similar experiment was conducted for feed concentration of 5 and 10 wt.% and the final concentrations are tabulated in Table 2.

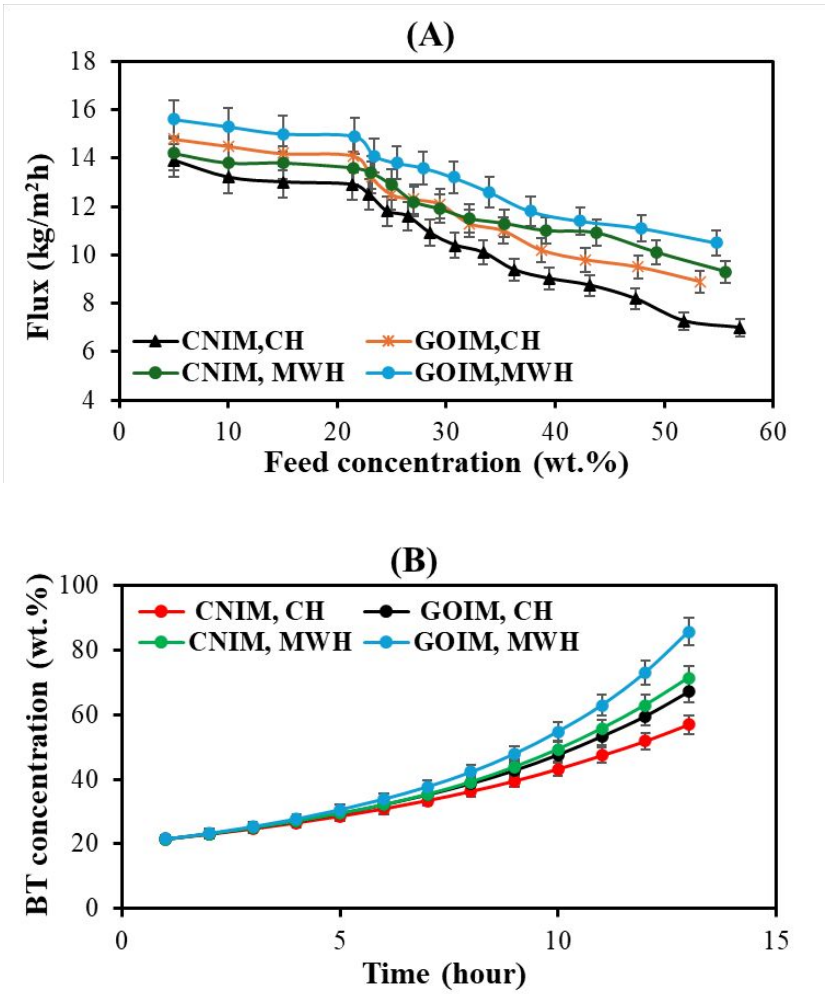

Figure 5. A) Change of flux as a function of feed concentration. B) Concentration as a function of time. Experiments were done at 80 °C under both heating methods at a flowrate of 100 mL/min.

The final concentration of the BT after MIMD is shown in Table 2. The initial feed concentration varied from 5 - 20 wt.% of BT. Initial concentration was 5 wt.% and after 13 h of distillation, the final concentration reached 29.2 wt.% for the CNIM membrane. The GOIM membrane showed further concentration enhancement to 34.1 wt.%. The incorporation of microwave irradiation improved the flux and raised the final feed concentration to 35.1 and 39.0 wt.% for the CNIM and GOIM membranes, respectively.

Table 2: Final BT concentration for both CNIM and GOIM membranes using CH and MWH (MD duration, 13 hours; flowrate, 100 mL/min; and temperature, 80 °C)

Membrane	Initial Feed (wt.%)	Final Feed (wt.%)	
		CH	MWH
CNIM	5	29.2	34.1
	10	42.9	44.9
	20	57	67.1
GOIM	5	35.1	39
	10	51.1	58
	20	71.3	85.7

A similar trend was observed for the experiments with initial concentrations of 10 and 20 wt.% BT. The 10 wt.% feed was concentrated to 51.1 wt.% using the CNIM membrane and 58 wt.% for the GOIM membrane. Meanwhile, the 20 wt.% feed was concentrated to 71.3% for the CNIM membrane and 85.7 wt.% for the GOIM membrane. The final concentration is dependent on efficient distillation and MIMD offers a higher dehydration rate. The experimental water flux suggests that microwave-based dehydration is more effective in concentrating the initial feed. The final feed becomes very dense and viscous with no phase separation. Figure 6 shows the comparison of initial and final feed in terms of physical appearance.

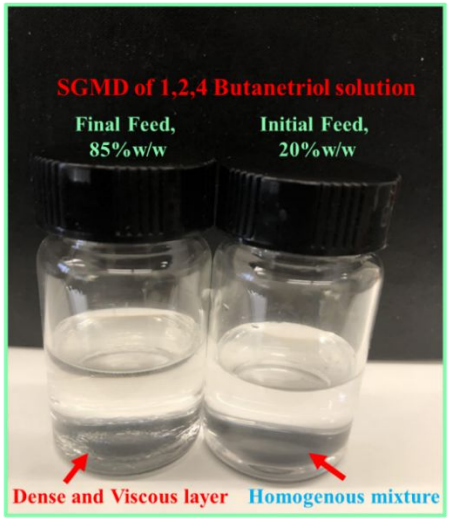

Figure 6. Physical appearance of the 1,2,4-butanetriol mixtures.

3.3. Mass transfer coefficient

The mass transfer coefficient (MTC) for the MD using BT mixtures is shown in Figure 7, and percentage change in MTC due to microwave irradiation at various concentrations is shown in Figure 8. The MTC represents the rate at which mass is transferred through the membrane per unit area, and it depends on various factors encompassing membrane properties, temperature, and feed properties. The relationship between overall MTC (k) and membrane flux (J) is shown in Eq. 2. Here P_f is the feed side vapor pressure and P_p is the permeate side vapor pressure. The vapor pressures of water were calculated using the Antoine equation. k values are important to explain permeation of water through membrane pores.

$$k = J/(P_f - P_p) \quad \text{..... (2)}$$

From Figure 7, it is evident the MTC is the highest at the onset of distillation when the concentration of BT is lower. Permeate flux drops as the feed side becomes more concentrated. At the highest concentration tested, the MTC dropped by almost 35% compared to the initial MTC. This reduction is attributed to the increased viscosity of the feed solution. The viscosity of the

solution increases with BT concentration increment. The flux of water dehydration reduced due to the increased viscosity shown in Figure 9-A. At 5 wt.% BT, the viscosity was 0.95 mPa.s whereas at 35 wt.%, the viscosity increased to 2.36 mPa.s. The viscosity at 25 ℃ is three times to the viscosity at 80 ℃. However, viscosity showed an increasing trend at higher concentrations and the increase in viscosity was considerable. The mass transfer variation as a function of viscosity is shown in Figure 9-B. Elevated viscosity impedes molecular movement, diminishing mass transfer efficiency in more viscous fluids. Viscosity's impact extends to diffusion rates as well, with more viscous fluids exhibiting slower diffusion, leading to an overall reduction in mass transfer rates. The application of microwave irradiation significantly improved the MTC. The change in MTC due to microwave irradiation (see Figure 8) provides further support for the role of microwave irradiation in increasing the efficiency of BT distillation. This effect is due to the breakdown of water-BT clusters and localized heating. The breakdown mechanism is graphically depicted in the coming session. The disruption of hydrogen bonding enables water molecules to disassociate and move through the membrane pores. In addition, the localized heating minimizes the boundary layer on the membrane-liquid interface.

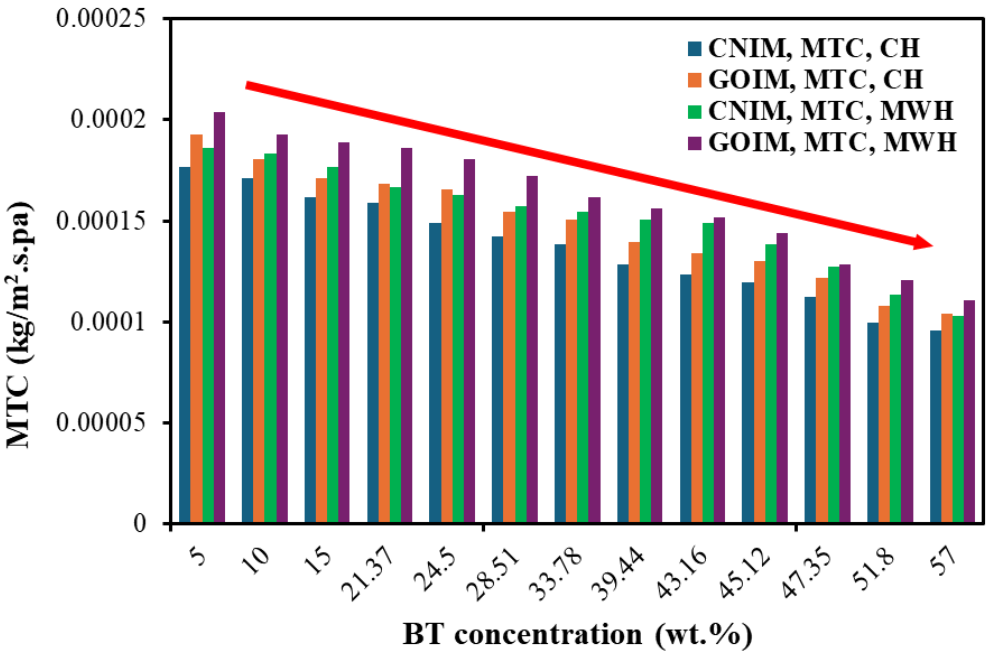

Figure 7. MTC with respect to concentration for GOIM and CNIM membranes.

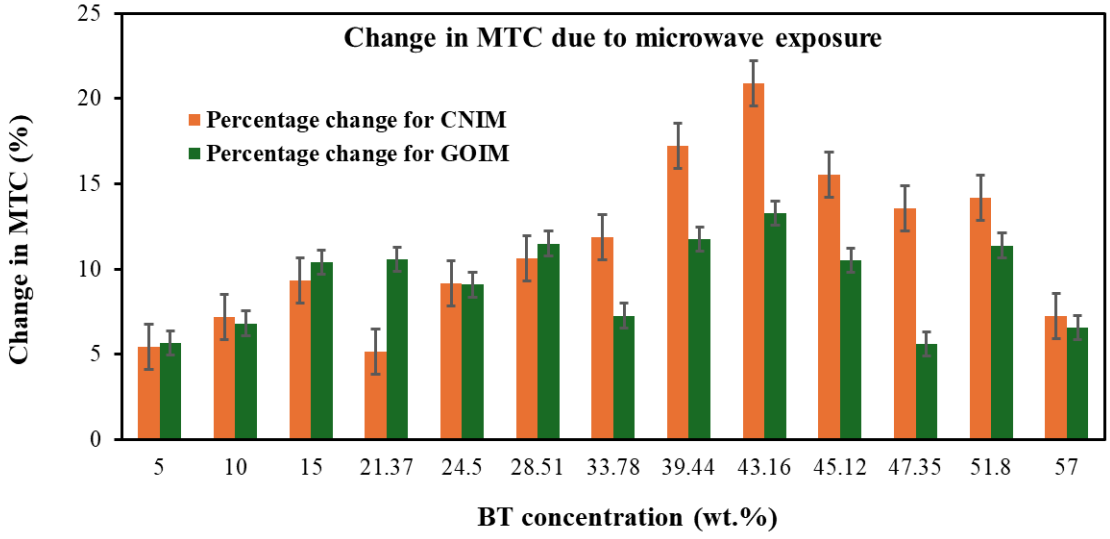

Figure 8. Change in MTC due to microwave exposure.

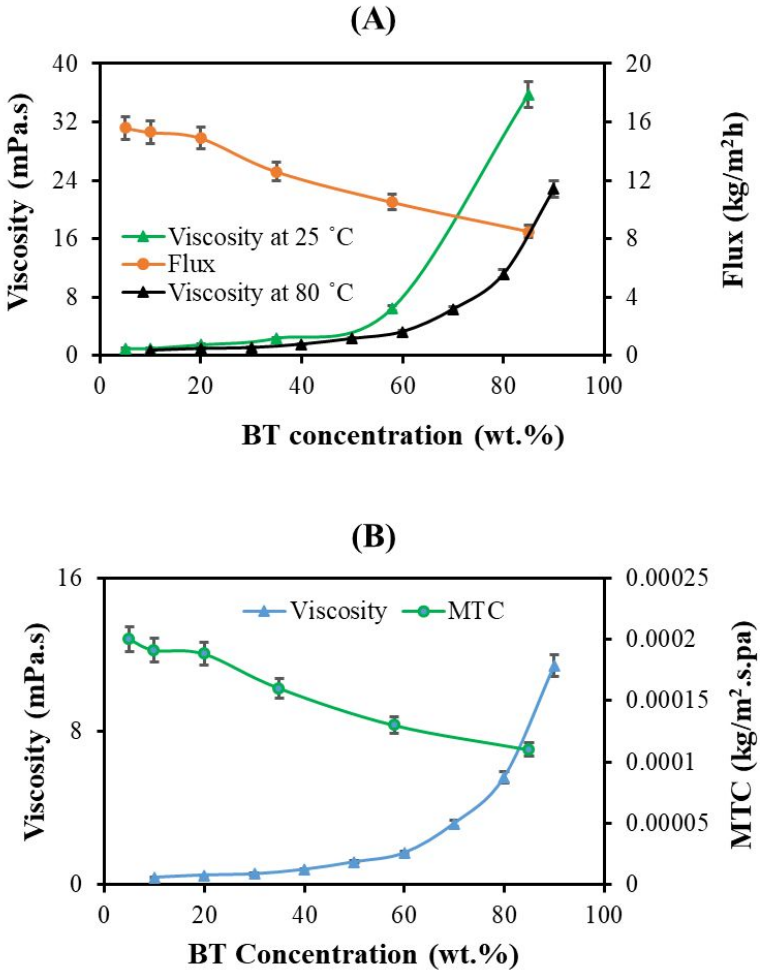

Figure 9. Effect of viscosity on the flux and mass transfer coefficient: (A) Flux as a function of viscosity; (B) MTC as a function of viscosity.

3.4. Dehydration mechanism

The proposed transport mechanism of water-BT cluster breakdown and permeation of water vapor through the membrane is shown in Figures 10 and 11. Microwave exposure preferentially heats up water molecules more compared to BT and exerts excitation energy to disrupt hydrogen bonding. The water molecules then move through the membrane based on the preferential sorption pathway promoted by the functional sites of CNIM and GOIM. As GOIM

has more functional groups in its structure, the permeation rate is higher for this membrane, resulting in more efficient concentration of the feed.

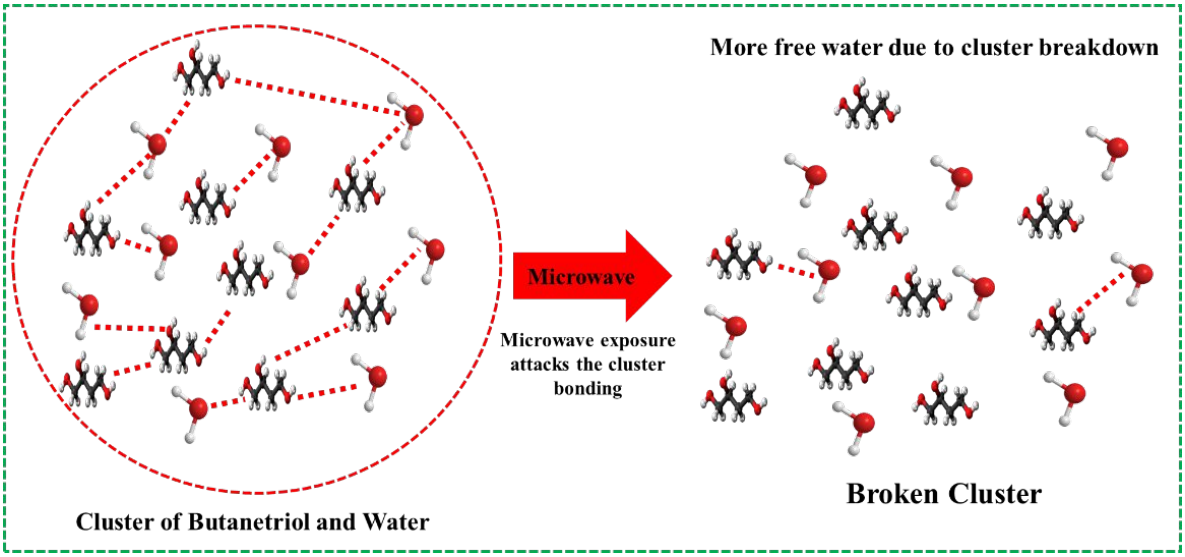

Figure 10. Breakdown of BT-water clusters due to microwave irradiation.

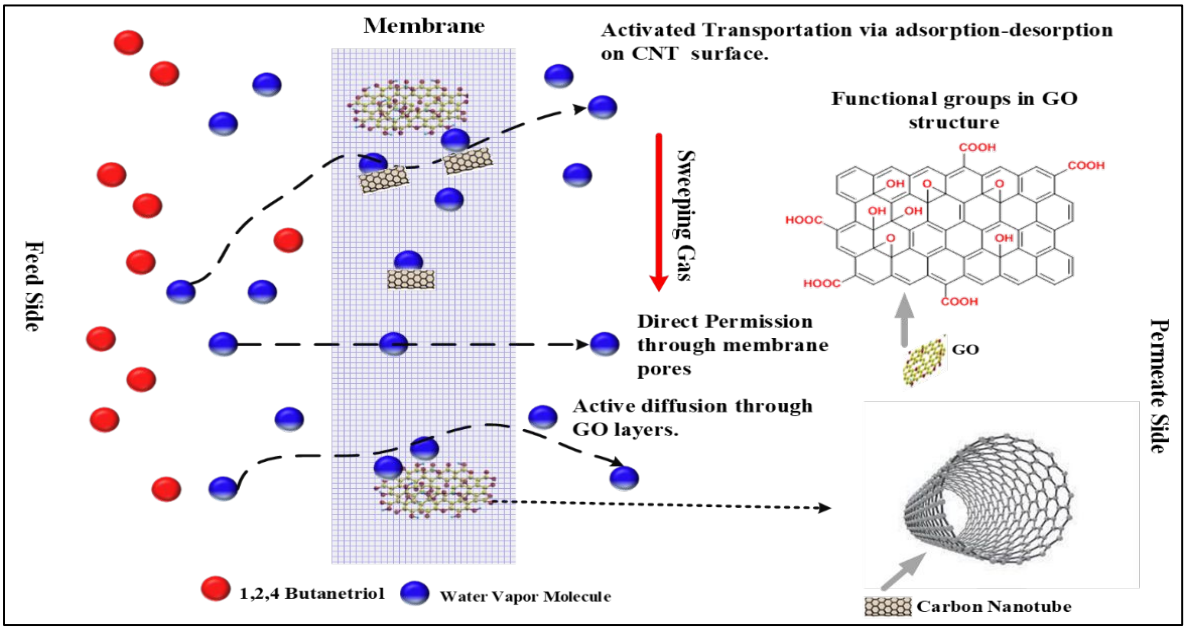

Figure 11. Water vapor transport mechanism in SGMD using GOIM and CNIM membranes.

3.5. Energy efficiency of BT dehydration by conventional MD and MIMD

Thermal analysis demonstrates the efficiency of the MD systems. There are several parameters that can be used to determine energy efficiency, namely evaporation efficiency and specific energy consumption. Evaporation efficiency is defined by the amount of heat utilized for flux compared to total energy passing through the membrane. Meanwhile, specific energy consumption shows how much energy is required per unit flux. The mathematical expression for each of the thermal efficiency parameters are given below:

$$\text{TE (\%)} = \frac{J_p \ A\Delta H_{v,w}}{Q_m} x\ 100 = \frac{Q_{vap}}{Q_{vap} + Q_{cond}} \text{ x 100} \ldots\ldots\ldots\ldots\ldots (3)$$

where Q_m is the heat transferred through the membrane by conduction and convection, J_p is the flux, A is the active membrane surface area, and H_v is the heat of vaporization for water. Heat transferring through the membrane can be calculated by Eq. 4, where m_f is the feed flow rate and C_p is the heat capacity of the water.

$$Q_m = m_f C_p (T_{f,\,in} - T_{f,\,out}) \ldots\ldots\ldots\ldots\ldots\ldots (4)$$

Eq. 5 shows the formula for calculating specific energy consumption (SEC) as follows:

$$\text{SEC (kWh/m}^3\text{)} = \left[\frac{Q_m \rho}{J_p A}\right] / 3600 \ldots\ldots\ldots\ldots\ldots (5)$$

Several assumptions were made to calculate thermal efficiency and specific energy consumption. For simplicity, the heat capacity of water was used for the feed. Also, membrane conductivity was taken as the base membrane conductivity. This is because only a small amount of nanocarbon is used for the modification of the membranes. The thermal efficiency for the MIMD of BT using CNIM and GOIM membranes is shown in Table 3. The evaporation efficiency of the system was quite high at 71% and 74.5% for the CNIM and GOIM membranes, respectively.

The specific energy consumption reduced for microwave heating. The GOIM membrane exhibited an SEC value of 263 kWh/m^3 for the microwave heated distillation of BT.

Table 3. Thermal efficiency and SEC of the membranes using CH and MWH.

Membrane	Thermal efficiency (%)		SEC (kWh/m^3)	
	CH	MWH	CH	MWH
CNIM	63	71	287	267
GOIM	66	74.5	281	263

4. Conclusion

In summary, microwave-assisted SGMD stands out as a promising and efficient method for concentrating BT in aqueous solutions in spite of high viscosity because of concentration increment. Utilizing CNIM and GOIM membranes, this approach surpasses traditional distillation techniques with its lower specific energy consumption, decreased operational expenses, and enhanced concentration of BT. Since the amount of CNT or GO used in membrane fabrication was very small, they do not significantly add to the overall cost of the membranes, making them economically viable options. Microwave-assisted SGMD enabled a final concentration of 85.7% from an initial feed solution of 20%. This process ensures efficient distillation with improved flux, while microwave irradiation further enhances thermal efficiency. Overall, microwave-assisted SGMD presents a promising method for efficient separation processes, offering significant benefits over conventional methods in terms of energy consumption, operational costs, and concentration enhancement of BT.

Conflict of Interest

The authors declare no conflict of interest.

Acknowledgement

This study was partially supported by a research award from the Naval Air Warfare Center, Weapons Division (Contract #N6893623P0424). BGH gratefully acknowledges support from the Strategic Environmental Research and Development Program (SERDP WP20-1391).

References

1. Huang, H. J.; Ramaswamy, S.; Al-Dajani, W. W.; Tschirner, U., Process modeling and analysis of pulp mill-based integrated biorefinery with hemicellulose pre-extraction for ethanol production: a comparative study. *Bioresour Technol* **2010,** *101* (2), 624-31.
2. Chen, H.; Cai, D.; Chen, C.; Zhang, C.; Wang, J.; Qin, P., Techno-economic analysis of acetone-butanol-ethanol distillation sequences feeding the biphasic condensate after in situ gas stripping separation. *Separation and Purification Technology* **2019,** *219*, 241-248.
3. Energy, U. D. o. *Top Value Added Chemicals from Biomass Volume I—Results of Screening for Potential Candidates from Sugars and Synthesis Gas.*; NREL: 2004.
4. Meng, Q.; Yu, J.; Yang, L.; Li, Y.; Xian, M.; Liu, H., Efficient recovery of bio-based 1,2,4-butanetriol by using boronic acid anionic reactive extraction. *Separation and Purification Technology* **2021,** *255*, 117728.
5. Romero, C. M.; Páez, M. S.; Lamprecht, I., Enthalpies of dilution of aqueous solutions of n-butanol, butanediols, 1,2,4-butanetriol, and 1,2,3,4-butanetetrol at 298.15K. *Thermochimica Acta* **2005,** *437* (1-2), 26-29.

6. Mao, X.; Qian, X.; Lin, J.; Wei, D., Engineering Gluconobacter oxydans for Efficient production of 3,4-dihydroxybutunate or 1,2,4-butanetriol from D-xylose. *Biochemical Engineering Journal* **2023,** *195*, 108936.
7. Tian, M.; Wu, S.-j.; Tian, X.-W.; Yao, D.-S.; Li, C.-L.; Hu, J.-S.; Zhang, B.-Y., Mesomorphic properties of chiral three-arm liquid crystals containing 1,2,4-butanetriol as core. *Journal of Molecular Structure* **2016,** *1107*, 202-213.
8. Kim, S.; Im, H.; Yu, J.; Kim, K.; Kim, M.; Lee, T., Biofuel production from Euglena: Current status and techno-economic perspectives. *Bioresour Technol* **2023,** *371*, 128582.
9. Velvizhi, G.; Jacqueline, P. J.; Shetti, N. P.; K, L.; Mohanakrishna, G.; Aminabhavi, T. M., Emerging trends and advances in valorization of lignocellulosic biomass to biofuels. *J Environ Manage* **2023,** *345*, 118527.
10. Joseph Antony Sundarsingh, T.; Ameen, F.; Ranjitha, J.; Raghavan, S.; Shankar, V., Engineering microbes for sustainable biofuel production and extraction of lipids – Current research and future perspectives. *Fuel* **2024,** *355*, 129532.
11. Khoo, K. S.; Ahmad, I.; Chew, K. W.; Iwamoto, K.; Bhatnagar, A.; Show, P. L., Enhanced microalgal lipid production for biofuel using different strategies including genetic modification of microalgae: A review. *Progress in Energy and Combustion Science* **2023,** *96*, 101071.
12. Mujtaba, M.; Fernandes Fraceto, L.; Fazeli, M.; Mukherjee, S.; Savassa, S. M.; Araujo de Medeiros, G.; do Espírito Santo Pereira, A.; Mancini, S. D.; Lipponen, J.; Vilaplana, F., Lignocellulosic biomass from agricultural waste to the circular economy: a review with focus on biofuels, biocomposites and bioplastics. *Journal of Cleaner Production* **2023,** *402*, 136815.

13. Zhang, N.; Wang, J.; Zhang, Y.; Gao, H., Metabolic pathway optimization for biosynthesis of 1,2,4-butanetriol from xylose by engineered Escherichia coli. *Enzyme Microb Technol* **2016,** *93-94*, 51-58.
14. Jing, P.; Cao, X.; Lu, X.; Zong, H.; Zhuge, B., Modification of an engineered Escherichia coli by a combined strategy of deleting branch pathway, fine-tuning xylose isomerase expression, and substituting decarboxylase to improve 1,2,4-butanetriol production. *J Biosci Bioeng* **2018,** *126* (5), 547-552.
15. Bamba, T.; Yukawa, T.; Guirimand, G.; Inokuma, K.; Sasaki, K.; Hasunuma, T.; Kondo, A., Production of 1,2,4-butanetriol from xylose by Saccharomyces cerevisiae through Fe metabolic engineering. *Metab Eng* **2019,** *56*, 17-27.
16. Wang, Z.; Kou, J.; Cao, Y.; Wang, X.; Xu, S.; Wu, J.; Lv, H.; Chen, K., Transient modeling of column adsorption–desorption processes for pre-concentration of D-1,2,4-butanetriol. *Separation and Purification Technology* **2021,** *275*, 118674.
17. Dahman, Y.; Syed, K.; Begum, S.; Roy, P.; Mohtasebi, B., Biofuels: Their characteristics and analysis. In *Biomass, biopolymer-based materials, and bioenergy*, Elsevier: 2019; pp 277-325.
18. Smallwood, I. M., *Solvent recovery handbook*. CRC Press: 2002.
19. Connor, M. R.; Atsumi, S., Synthetic biology guides biofuel production. *BioMed Research International* **2010,** *2010*.
20. Mitra, S. P. a. S., Carbon Nanotube Enhanced Membrane Filtration for Dewatering of Butanol. *Separation and Purification Technology* **2023**, In review.
21. Paul, S., Stein, L., Salemi, A.,and S. Mitra, , Development of Omniphobic coating for Biomedical Devices; In Review. . *Industrial and Engr. Chemistry* **2023**, In Review.

22. Bindels, M.; Medaer, B.; Gebrehiwot, M.; Nelemans, B., Approximation of dynamic membrane distillation processes applied to concentration of aqueous sucrose solutions. *Desalination* **2021,** *503*, 114951.
23. Moejes, S. N.; van Wonderen, G. J.; Bitter, J. H.; van Boxtel, A. J. B., Assessment of air gap membrane distillation for milk concentration. *Journal of Membrane Science* **2020,** *594*, 117403.
24. Khiter, A.; Balannec, B.; Szymczyk, A.; Arous, O.; Nasrallah, N.; Loulergue, P., Behavior of volatile compounds in membrane distillation: The case of carboxylic acids. *Journal of Membrane Science* **2020,** *612*, 118453.
25. Skuse, C.; Gallego-Schmid, A.; Azapagic, A.; Gorgojo, P., Can emerging membrane-based desalination technologies replace reverse osmosis? *Desalination* **2021,** *500*, 114844.
26. Xu, Y.; Yang, Y.; Fan, X.; Liu, Z.; Song, Y.; Wang, Y.; Tao, P.; Song, C.; Shao, M., In-situ silica nanoparticle assembly technique to develop an omniphobic membrane for durable membrane distillation. *Desalination* **2021,** *499*, 114832.
27. Shaulsky, E.; Wang, Z.; Deshmukh, A.; Karanikola, V.; Elimelech, M., Membrane distillation assisted by heat pump for improved desalination energy efficiency. *Desalination* **2020,** *496*, 114694.
28. Bin Bandar, K.; Alsubei, M. D.; Aljlil, S. A.; Bin Darwish, N.; Hilal, N., Membrane distillation process application using a novel ceramic membrane for Brackish water desalination. *Desalination* **2021,** *500*, 114906.
29. Zuo, K.; Wang, W.; Deshmukh, A.; Jia, S.; Guo, H.; Xin, R.; Elimelech, M.; Ajayan, P. M.; Lou, J.; Li, Q., Multifunctional nanocoated membranes for high-rate electrothermal desalination of hypersaline waters. *Nat Nanotechnol* **2020,** *15* (12), 1025-1032.

30. Roy, S.; Ragunath, S., Emerging Membrane Technologies for Water and Energy Sustainability: Future Prospects, Constrains and Challenges. *Energies* **2018,** *11* (11), 2997.
31. Mitun Chandra Bhoumick, S. R., Somenath Mitra *, Enrichment of 1, 4-dioxane from water by sweep gas membrane distillation on nano-carbon immobilized membranes. *Separation and Purification Technology* **2021**.
32. Intrchom, W.; Roy, S.; Mitra, S., Functionalized carbon nanotube immobilized membrane for low temperature ammonia removal via membrane distillation. *Separation and Purification Technology* **2020,** *235*, 116188.
33. Intrchom, W.; Roy, S.; Humoud, M. S.; Mitra, S., Immobilization of Graphene Oxide on the Permeate Side of a Membrane Distillation Membrane to Enhance Flux. *Membranes (Basel)* **2018,** *8* (3).
34. Gupta, O.; Roy, S.; Mitra, S., Microwave Induced Membrane Distillation for Enhanced Ethanol–Water Separation on a Carbon Nanotube Immobilized Membrane. *Industrial & Engineering Chemistry Research* **2019,** *58* (39), 18313-18319.
35. Bhoumick, M. C.; Roy, S.; Mitra, S., Reduction and Elimination of Humic Acid Fouling in Air Sparged Membrane Distillation Using Nanocarbon Immobilized Membrane. *Molecules* **2022,** *27* (9).
36. Humoud, M. S.; Roy, S.; Mitra, S., Scaling Reduction in Carbon Nanotube-Immobilized Membrane during Membrane Distillation. *Water* **2019,** *11* (12), 2588.
37. Chandra Bhoumick, M.; Roy, S.; Mitra, S., Synergistic effect of air Sparging in Direct Contact Membrane Distillation to Control Membrane Fouling and Enhancing Flux. *Separation and Purification Technology* **2021**, 118681.

38. Gupta, I.; Azizighannad, S.; Farinas, E. T.; Mitra, S., Antiviral properties of select carbon nanostructures and their functionalized analogs. *Materials Today Communications* **2021,** *29*, 102743.

39. Gethard, K.; Sae-Khow, O.; Mitra, S., Carbon nanotube enhanced membrane distillation for simultaneous generation of pure water and concentrating pharmaceutical waste. *Separation and Purification Technology* **2012,** *90*, 239-245.

40. Paul, S.; Bhoumick, M. C.; Roy, S.; Mitra, S., Carbon nanotube enhanced membrane filtration for trace level dewatering of hydrocarbons. *Separation and Purification Technology* **2022,** *292*, 121047.

41. Bhadra, M.; Roy, S.; Mitra, S., Flux enhancement in direct contact membrane distillation by implementing carbon nanotube immobilized PTFE membrane. *Separation and Purification Technology* **2016,** *161*, 136-143.

42. Roy, S.; Humoud, M. S.; Intrchom, W.; Mitra, S., Microwave-Induced Desalination via Direct Contact Membrane Distillation. *ACS Sustainable Chemistry & Engineering* **2017,** *6* (1), 626-632.

43. Gupta, O.; Roy, S.; Mitra, S., Low temperature recovery of acetone–butanol–ethanol (ABE) fermentation products via microwave induced membrane distillation on carbon nanotube immobilized membranes. *Sustainable Energy & Fuels* **2020,** *4* (7), 3487-3499.

44. Gupta, O.; Roy, S.; Mitra, S., Nanocarbon-Immobilized Membranes for Separation of Tetrahydrofuran from Water via Membrane Distillation. *ACS Applied Nano Materials* **2020,** *3* (7), 6344-6353.

Dehydration of Highly Viscous Polyol (1,2,4-Butanetriol) Using Microwave-Induced Sweep Gas Membrane Distillation (MIMD) on Nanocarbon-Immobilized Membranes

Mitun Chandra Bhoumick[1], Benjamin G. Harvey[2], Derek D. Zhang[2], Somenath Mitra[1,*]

[1] Department of Chemistry and Environmental Science, New Jersey Institute of Technology, Newark, NJ 07102, USA

[2] US Navy, Naval Air Warfare Center, Weapons Division, Research Department, Chemistry Division, China Lake, CA 93555, USA

[*] Corresponding Author: Tel: 973-596-5611; Email: *Somenath.mitra@njit.edu*

Data availability

Data are available upon request from the authors.